

Programming Self-assembly of Virus-like Shells via Colloidal Bond Hybridization

Chris H.J. Evers, Jurriaan A. Luiken, Peter G. Bolhuis, Willem K. Kegel

March 27, 2025

Abstract

Colloids with directional interactions are promising building blocks for new functional materials and models for biological structures^{1,2,3}. Using rigid patches, for example, particles have been programmed to self-assemble into kagome lattices and colloidal equivalents of molecules and micelles^{4,5,6}. Self-assembly into more complex structures such as virus-like shells, however, requires more complex patch geometries⁷, which—to the best of our knowledge—have not been experimentally realized yet. Protein building blocks of real viruses, on the other hand, can undergo conformational changes upon self-assembly^{8,9}. Here we demonstrate, by combining experiments and simulations, that conformationally changeable colloids self-assemble into complex structures such as virus-like shells. These floppy colloids contain both mutually attractive and repulsive surface groups that are mobile. Analogous to the simplest chemical bond, where two isotropic orbitals hybridize into the molecular orbital of H_2 , these mobile groups redistribute upon binding. By introducing bond hybridization in the colloidal domain, we programmed relatively simple flexible building blocks to self-assemble into dramatically more complex structures than would have been anticipated based on their rigid geometry.

The simplest particle geometries for which we induce colloidal bond hybridization are cross-linked poly(styrene-*co*-acrylic acid) (CPSAA) spheres in water. Acrylic acid and styrene are incorporated at different stages in

the synthesis^{10,11}, and the poly(acrylic acid)-rich (pAA) brush can undergo a conformational change, rendering the particle deformable or ‘floppy’.

This structural rearrangement can be observed with Dynamic Light Scattering (DLS). For spheres with a Transmission Electron Microscopy diameter $d_{\text{TEM}} = 0.547 \pm 0.021 \mu\text{m}$, d_{DLS} equals $0.79 \mu\text{m}$ at pH 10, but decreases to $0.57 \mu\text{m}$ at pH 3 (Extended Data Fig. 1). For either higher salt concentrations, or for particles without acrylic acid, the size is almost constant. Hence, high pH induces electrostatic repulsion, and triggers the brush to expand $\mathcal{O}(0.1) \mu\text{m}$ into the solution.

In water without added salt, the floppy spheres self-assemble into planar sheets (Fig. 1). In the sheets, particles are hexagonally ordered in a monolayer that moves freely in the solution. We hypothesize that a colloidal equivalent of bond hybridization causes the observed planar directionality. The polymer brush contains both negatively charged acrylic acid groups, and mutually attractive styrene moieties. Upon binding, the brushes combine and the acrylic acid-rich and styrene-rich parts of floppy chains microphase separate inducing directional interactions (Fig. 1e).

This stabilizing mechanism is verified by Monte Carlo simulations. The colloid cores with hydrophobic moieties are modelled as mutually short-ranged attractive hard spheres with diameter σ and the hydrophilic chains as f mobile penetrable hard sphere Asakura-Oosawa particles^{12,13} of diameter $q\sigma$ attached to the surface (Fig. 1f). Starting from a hexagonal planar configuration, the particles reorganize into compact aggregates at low f and q to maximize the interparticle contacts. Upon increasing f and q , however, the polymers redistribute out of plane and mechanically stable bilayers and monolayers are observed (Fig. 1g-j).

We quantify the dimensionality of the resulting structures by the average number of contacts per particle, \bar{N}_c . By plotting \bar{N}_c as a function of the polymer surface fraction, $Q = \frac{fq^2}{4(q+1)^2}$ (SI 1), the curves for f and q collapse (Fig. 1k). For compact clusters, \bar{N}_c is lower than expected for a compact bulk configuration, because a large fraction of particles is at the surface of the clusters. Increasing Q lowers \bar{N}_c , implying a transition to lower dimensional structures.

Cooperative redistribution of polymers thus induces directional interactions for isotropic particles, and these observations are in line with experiments and simulations for polymer-grafted nanoparticles^{14,15,16}. DNA coated colloids can also form similar crystalline monolayers, but for these particles,

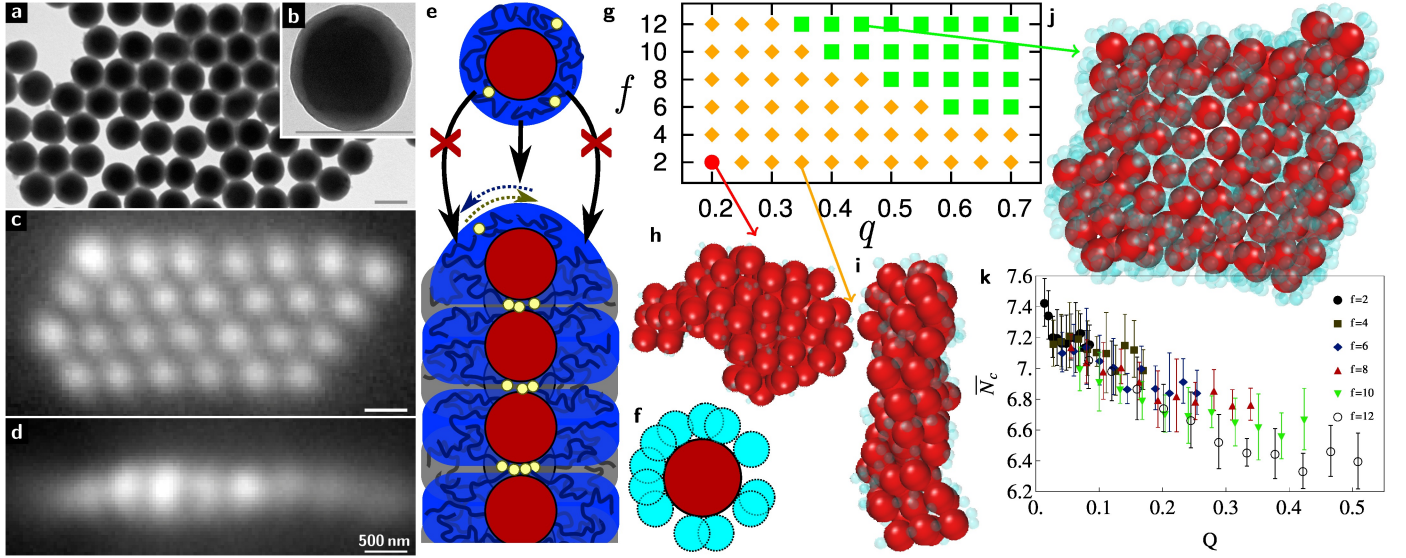


Figure 1: *Self-assembled planar sheets*. TEM image of floppy spheres (a-b) and reflectance microscopy images of self-assembled sheets (c, top) and (d, side). e) In colloidal bond hybridization, hydrophobic moieties (yellow) move towards the contact area, while hydrophilic chains (blue) move into the solution. f) Particles are simulated as attractive spheres of size σ (red) with f mobile penetrable hard spheres (blue) of size $q\sigma$. g) Depending on f and q , compact clusters (h), bilayers (i) and monolayers (j) are found. k) The average number of contacts, \bar{N}_c , decreases upon increasing the polymer surface fraction, Q . Error bars indicate s.d. for five independent simulations.

directional interactions are induced by a functionalized surface¹⁷.

Complexity increases upon breaking the symmetry of the building blocks, which induces self-assembly into hollow spherical shells (Fig. 2). We break the symmetry of the floppy spheres by protrusion formation^{18,19,20}. Next, we increase the brush hydrophobicity by functionalizing the acrylic acid groups²¹ and wash the particles by centrifugation. Finally, we obtain snowman-like particles with a floppy side and a hard side (Fig. 2a, Extended Data Fig. 2-3).

The shell configuration can be observed in dispersion with optical microscopy, and after sintering or freeze drying with Scanning Electron Microscopy (SEM) (Fig. 2i, Extended Data Fig. 4). The shells consist of a particle monolayer while the interior is water-filled (Fig. 2k). Furthermore, excess styrene is removed before shell formation occurs, so unlike colloidosomes²², here, no template is involved.

For particles with a body diameter, d_b , of 0.55 μm , the shell diameter varies from 3-5 μm , with $\mathcal{O}(10^2)$ particles per shell. Most particles have six nearest neighbors, but pentagons occur frequently to fill the spherical surface. However, no (icosahedral) symmetry is observed. Furthermore, most particle protrusions are pointing slightly out of plane, either inwards or outwards with respect to the center of the shell.

The self-assembly mechanism is robust, as both shells and sheets are found for snowman-like particles with d_b ranging from 454 to 645 nm, and for functionalization with *tert*-butylamine (tBA) or fluoresceinamine (FlA) (Fig. 2b-h, Extended Data Fig. 5). For CPSAA spheres, however, symmetry is unbroken, and increasing the hydrophobicity does not induce the formation of shells. For large functionalized snowman-like particles ($d_b = 894$ nm), the pAA chains are short compared to d_b and no shells are observed. Furthermore, for all particle sizes in Fig. 2, no shells are observed before hydrophobic functionalization. Hence, anisotropy, floppiness and hydrophobic functionalization all seem to be crucial for the observed directionality.

We add anisotropy to our Monte Carlo model by adding a protrusion, and the protrusion hydrophobicity is captured with a square well interaction. Starting with hexagonal sheets, stable monolayers are obtained by increasing Q (Fig. 2m-r). At moderate Q , both planar monolayers (Fig. 2n) and curved monolayers with protrusions pointing just out of plane (Fig. 2o-p) are observed. At even higher Q , all protrusions point inwards (Fig. 2q-r).

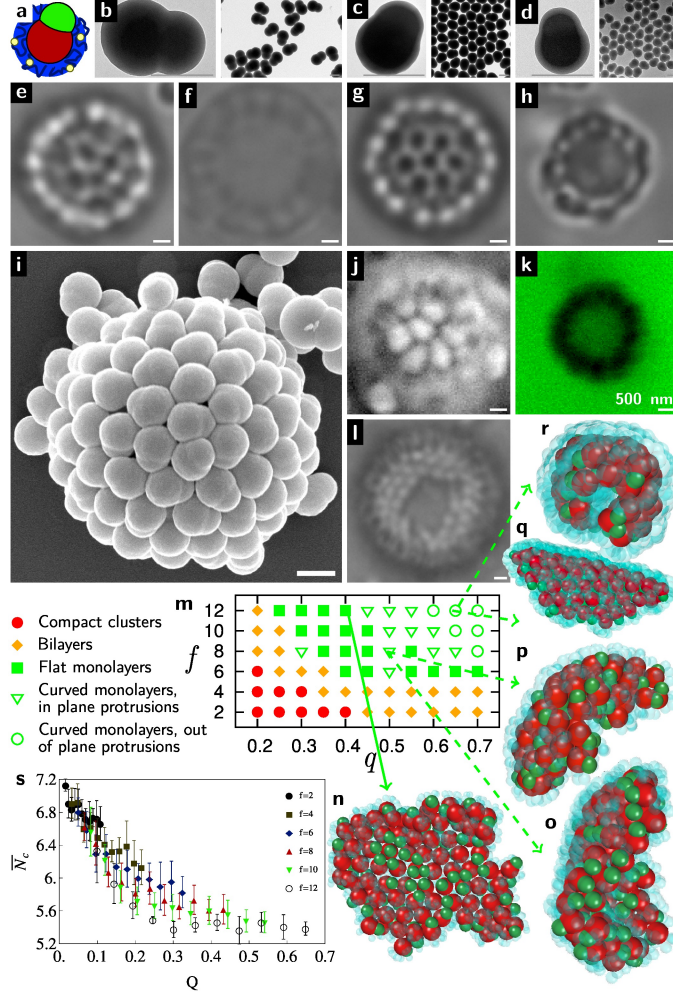


Figure 2: *Hollow self-assembled shells.* Snowman-like particles (a) with hydrophilic (blue) and hydrophobic (yellow) moieties are synthesized with varying sizes (b-d). For each size (f-h), and upon functionalization with both tBA (e) and FLA (f-l), self-assembled shells are found. SEM (i) and reflectance microscopy (j) show protrusions orient in plane, and dyeing the water phase (k) shows the shells are water-filled. l) a shell with stable vacancies. Simulations (m-s) show increasing curvature with the number, f , and size, $q\sigma$, of polymers, and n) dimensionality, \bar{N}_c , decreases with the polymer surface fraction, Q . Error bars indicate s.d. for five independent simulations.

For non-attractive protrusions, we also obtain curved monolayers, but now, for each f and q , protrusions are pointing inwards (data not shown). We conclude that protrusions break the symmetry of the sheets and induce curvature, stabilizing structures similar to the experimental shells. Upon starting simulations with free particles (Extended Data Fig. 6), dimensionality also decreases upon increasing Q , however, for neither spheres nor snowman-like particles monolayers are observed (Extended Data Fig. 7-8). This suggests that sheets and shells do not form spontaneously from a gaseous phase, but are the result of a more complex formation mechanism.

The formation mechanism becomes more clear by studying particles upon densification. At relatively high volume fractions, free snowman-like particles form a 'bubble phase' (Fig. 3i-m). In this highly fluctuating phase, microphase separation in dense and dilute regions occurs. Bond hybridisation prevents macroscopic phase separation, which is also illustrated by simulations for strong interparticle attractions (Extended Data Fig. 7-8).

Instead, dense curved structures around holes are observed. The curvature is probably induced by the protrusion, as protrusions also induce curvature of monolayers (Fig. 2o-r). The radii of the holes are comparable to the radii of the shells (Fig. 2), suggesting that the bubble phase is the first step in the formation mechanisms of the shells.

The next step in the formation mechanism is the formation of irreversible bonds. Particles in shells form strong bonds as no exchange is observed and the scarce vacancies are stable over days (Fig. 2l, Extended Data Fig. 9). Furthermore, the center-to-center-distance distribution peaks at $r_{ij} = 0.62 \mu\text{m}$ (Fig. 3n), which is just above twice the average edge-to-center-of-mass-distance per particle as determined by TEM. Free particles, however, form weak bonds at a $0.1 \mu\text{m}$ larger distance (Fig. 3n-o). Probably, the $0.1 \mu\text{m}$ floppy brush prevents free particles to form stable bonds, while self-assembled particles have penetrated the brush to reach the Van der Waals minimum. The effective force to penetrate the brush, about $30k_B T/\mu\text{m}$ (Fig. 3o), is comparable with the sedimentation force upon centrifugation, so centrifugation likely induces the second step in the formation mechanism.

A dense phase with holes is also observed in an evaporating droplet (Fig. 3a-h). Here, densification is induced by the solvent flow towards the glass/water/air contact line²³. At the glass slide near the contact line, a dense monolayer is formed with circular holes. and also in this case, the radii

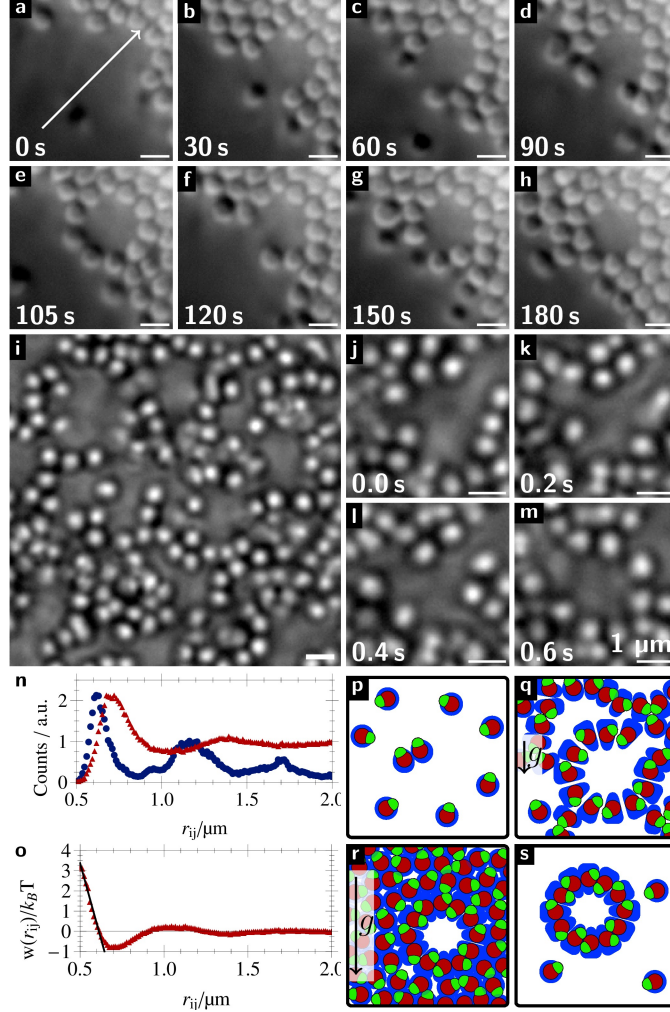


Figure 3: *Structure formation upon densification.* Circular structure formation in an evaporating droplet (a-h) and a highly fluctuating ‘bubble phase’ (i-m). The arrow indicates the evaporation direction. n) Normalized histograms of the interparticle distance peak at $0.72\mu\text{m}$ (bubble phase, red, triangles), and at $0.62\mu\text{m}$ (shells, blue, spheres), while the snowman-like particles have a body diameter of $0.55\mu\text{m}$. o) The associated bulk effective pair potential and a linear fit of the repulsive regime. p-s) Proposed formation mechanism: free particles (p) form a bubble phase in the gravitational field (q), and are pushed into close contact upon sedimentation. Upon redispersion (s), particles that surrounded holes are found as shells.

of the holes are comparable to the radii of the shells (Fig. 2). Here, however, liquid flow might also have an effect.

Based on these observation, we propose that colloidal bond hybridization combined with centrifugation drives the self-assembly (Fig. 3p-s). Upon centrifugation, the concentration increases gradually, and first a bubble phase with holes is formed. Next, particles are pushed into their primary minimum at even higher concentrations. Finally, after redispersion, particles that surrounded the holes are found as shells in the dispersion.

This mechanism is an example of two-step assembly, which involves first alignment and then bond formation. Activated assembly can also be found in nanocrystal superlattice assembly, where the interface orients particles before atomic binding occurs²⁴, and protein assembly, where often ATP forms covalent bonds after alignment⁹. In our system, gravity induces irreversible bond formation and for the first time to our knowledge, colloidal spherical virus-like structures are self-assembled without a template. Furthermore, a conformational change upon binding globally mimics protein self-assembly^{8,9}. Unlike previous work on soft nanoparticles that alter their valence after changing the solvent²⁵, here, many body interactions determine the valence at the moment particles bind. This mechanism is also fundamentally different from previous work on patchy particles and on ellipsoids that assemble into microtubules in an electric field²⁶.

Introducing bond hybridization in the colloidal domain allows programming simple building blocks to self-assemble into complex structures, whereas for rigid patchy particles, the number of required patches increases dramatically with the complexity of the desired structures. To the best of our knowledge, hollow self-assembled shells, for example, have only been predicted using rigid patches for cone-shaped particles with four different patches⁷, a system not experimentally realized yet.

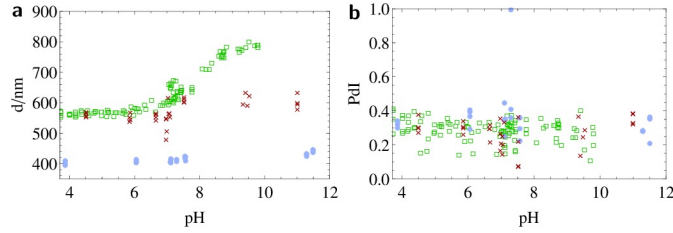
In colloidal bond hybridization, directional interactions emerge from a competition between excluded volume effects and hydrophobic attraction, but a novel theoretical framework is needed to predict into what structures particles self-assemble. Quantification of properties such as softness, attraction strength, asymmetry and number of patches lead to an enormous parameter space that remains to be explored. Independently controlling these parameters, however, remains a challenge that needs to be systematically addressed.

References

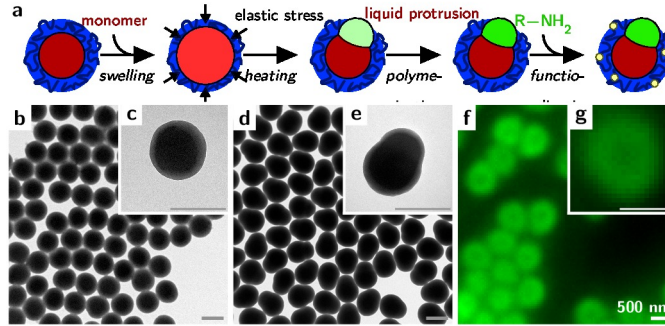
1. Zhang, Z. & Glotzer, S. C. Self-Assembly of Patchy Particles. *Nano Letters* **4**, 1407–1413 (2004). URL <http://dx.doi.org/10.1021/nl0493500>.
2. Glotzer, S. C. & Solomon, M. J. Anisotropy of building blocks and their assembly into complex structures. *Nature materials* **6**, 557–562 (2007).
3. Yi, G.-R., Pine, D. J. & Sacanna, S. Recent progress on patchy colloids and their self-assembly. *Journal of Physics: Condensed Matter* **25**, 193101 (2013). URL <http://stacks.iop.org/0953-8984/25/i=19/a=193101>.
4. Chen, Q., Bae, S. C. & Granick, S. Directed self-assembly of a colloidal kagome lattice. *Nature* **469**, 381–384 (2011). URL <http://www.ncbi.nlm.nih.gov/pubmed/21248847>.
5. Wang, Y. *et al.* Colloids with valence and specific directional bonding. *Nature* **491**, 51–55 (2012). URL <http://dx.doi.org/10.1038/nature11564>.
6. Kraft, D. J. *et al.* From the Cover: Surface roughness directed self-assembly of patchy particles into colloidal micelles. *Proceedings of the National Academy of Sciences* **109**, 10787–10792 (2012). URL <http://www.pnas.org/content/109/27/10787.abstract>.
7. Chen, T., Zhang, Z. & Glotzer, S. C. Simulation studies of the self-assembly of cone-shaped particles. *Langmuir* **23**, 6598–6605 (2007). 0608613.
8. Freund, S. M. V., Johnson, C. M., Jaulent, A. M. & Ferguson, N. Moving towards High-Resolution Descriptions of the Molecular Interactions and Structural Rearrangements of the Human Hepatitis B Core Protein. *Journal of Molecular Biology* **384**, 1301–1313 (2008). URL <http://www.sciencedirect.com/science/article/pii/S0022283608012928>.
9. Berg, J. M., Tymoczko, J. L. & Stryer, L. *Biochemistry* (W. H. Freeman and Company: New York, 2002).

10. Wang, P. H. & Pan, C.-Y. Preparation of styrene/acrylic acid copolymer microspheres: polymerization mechanism and carboxyl group distribution. *Colloid & Polymer Science* **280**, 152–159 (2002). URL <http://dx.doi.org/10.1007/s003960100588>.
11. Hu, X., Liu, H., Ge, X., Yang, S. & Ge, X. Preparation of Submicron-sized Snowman-like Polystyrene Particles via Radiation-induced Seeded Emulsion Polymerization. *Chemistry Letters* **38**, 854–855 (2009).
12. Asakura, S. & Oosawa, F. On interaction between two bodies immersed in a solution of macromolecules. *The Journal of Chemical Physics* **22**, 1255 (1954).
13. Vrij, a. Polymers at Interfaces and the Interactions in Colloidal Dispersions. *Pure and Applied Chemistry* **48**, 471–483 (1976).
14. Akcora, P. *et al.* Anisotropic self-assembly of spherical polymer-grafted nanoparticles. *Nature Materials* **8**, 354–359 (2009). URL <http://dx.doi.org/10.1038/nmat2404>http://www.nature.com/nmat/journal/v8/n4/supinfo/nmat2404_S1.html.
15. Nikolic, M. S. *et al.* Micelle and Vesicle Formation of Amphiphilic Nanoparticles. *Angewandte Chemie International Edition* **48**, 2752–2754 (2009). URL <http://dx.doi.org/10.1002/anie.200805158>.
16. Luiken, J. A. & Bolhuis, P. G. Anisotropic aggregation in a simple model of isotropically polymer-coated nanoparticles. *Physical Review E* **88**, 012303 (2013). URL <http://link.aps.org/doi/10.1103/PhysRevE.88.012303>.
17. Geerts, N. & Eiser, E. Flying colloidal carpets. *Soft Matter* **6**, 664–669 (2010). URL <http://dx.doi.org/10.1039/B917846E>.
18. Sheu, H. R., El-Aasser, M. S. & Vanderhoff, J. W. Uniform nonspherical latex particles as model interpenetrating polymer networks. *Journal of Polymer Science Part A: Polymer Chemistry* **28**, 653–667 (1990). URL <http://dx.doi.org/10.1002/pola.1990.080280315>.
19. Mock, E. B., De Bruyn, H., Hawket, B. S., Gilbert, R. G. & Zukoski, C. F. Synthesis of Anisotropic Nanoparticles by Seeded Emulsion Polymerization. *Langmuir* **22**, 4037–4043 (2006). URL <http://pubs.acs.org/doi/abs/10.1021/la060003a>.

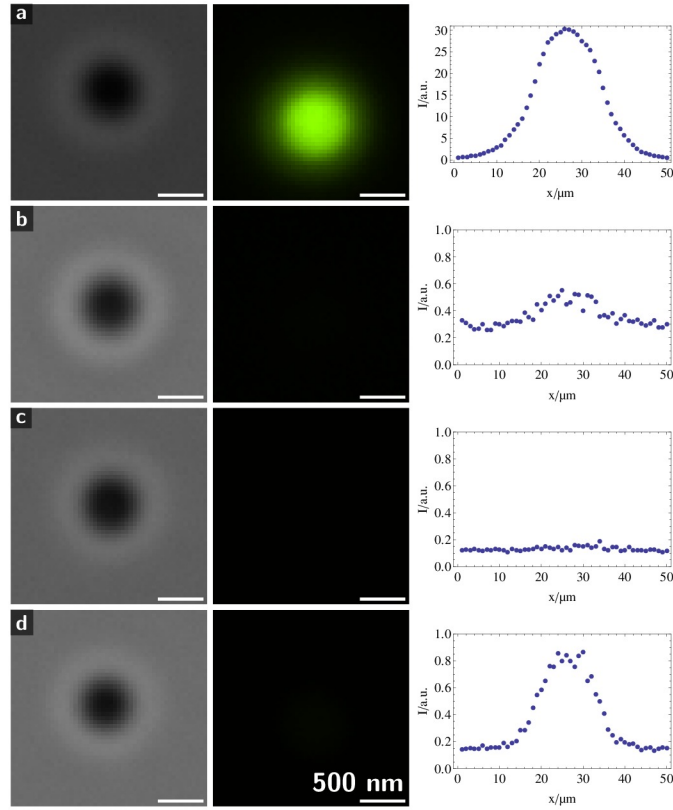
20. Kraft, D. J., Groenewold, J. & Kegel, W. K. Colloidal molecules with well-controlled bond angles. *Soft Matter* **5**, 3823–3826 (2009).
21. Marchand-Brynaert, J., Deldime, M., Dupont, I., Dewez, J.-L. & Schneider, Y.-J. Surface Functionalization of Poly(ethylene terephthalate) Film and Membrane by Controlled Wet Chemistry: Chemical Characterization of Carboxylated Surfaces. *Journal of Colloid and Interface Science* **173**, 236–244 (1995). URL <http://www.sciencedirect.com/science/article/pii/S0021979785713197>.
22. Dinsmore, A. D. *et al.* Colloidosomes: selectively permeable capsules composed of colloidal particles. *Science* **298**, 1006–1009 (2002). URL <http://www.ncbi.nlm.nih.gov/pubmed/12411700>.
23. Deegan, R. D. *et al.* Capillary flow as the cause of ring stains from dried liquid drops. *Nature* **389**, 827–829 (1997). URL <http://dx.doi.org/10.1038/39827>.
24. Evers, W. H. *et al.* Low-Dimensional Semiconductor Superlattices Formed by Geometric Control over Nanocrystal Attachment. *Nano Letters* **13**, 2317–2323 (2013). URL <http://dx.doi.org/10.1021/nl303322k>.
25. Groschel, A. H. *et al.* Guided hierarchical co-assembly of soft patchy nanoparticles. *Nature* **503**, 247–251 (2013). URL <http://dx.doi.org/10.1038/nature12610>.
26. Crassous, J. J. *et al.* Field-induced assembly of colloidal ellipsoids into well-defined microtubules. *Nature communications* **5**, 5516 (2014).



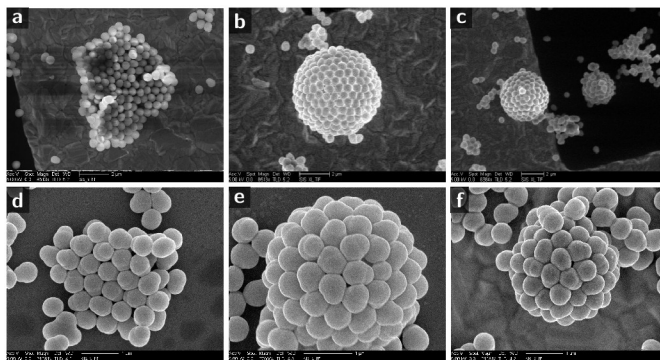
Extended Data Figure 1: *pH-induced conformational change*. Upon decreasing pH from 9.8 to 3.4 at ionic strength $I = 1$ mM, the apparent DLS diameter of CPSAA spheres decreases from 0.79 to 0.57 μm (left, green open squares), while the measured polydispersity index stays constants (right), indicating that pH does not influence aggregation. For CPSAA spheres at $I = 10$ mM (red crosses), electrostatic interaction are screened and the pH dependence is much smaller, indicating that electrostatic repulsion causes the size dependence. For CPS spheres at $I = 1$ mM (blue filled circles), the apparent diameter is also constant, suggesting that protonation of carboxylic acid groups at low pH induces the conformational change.



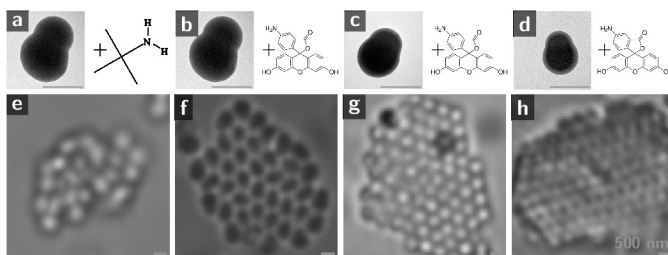
Extended Data Figure 2: Schematic outline (a) and microscopy images of the synthesis steps. Poly(styrene-*co*-acrylic acid) spheres (b-c) are swollen with monomer, heated, and polymerized, resulting in snowman-like particles (d-e). Hydrophobic molecules are covalently linked to the carboxylic acid groups, resulting in fluorescent particles after fluoresceinamine binding (f-g).



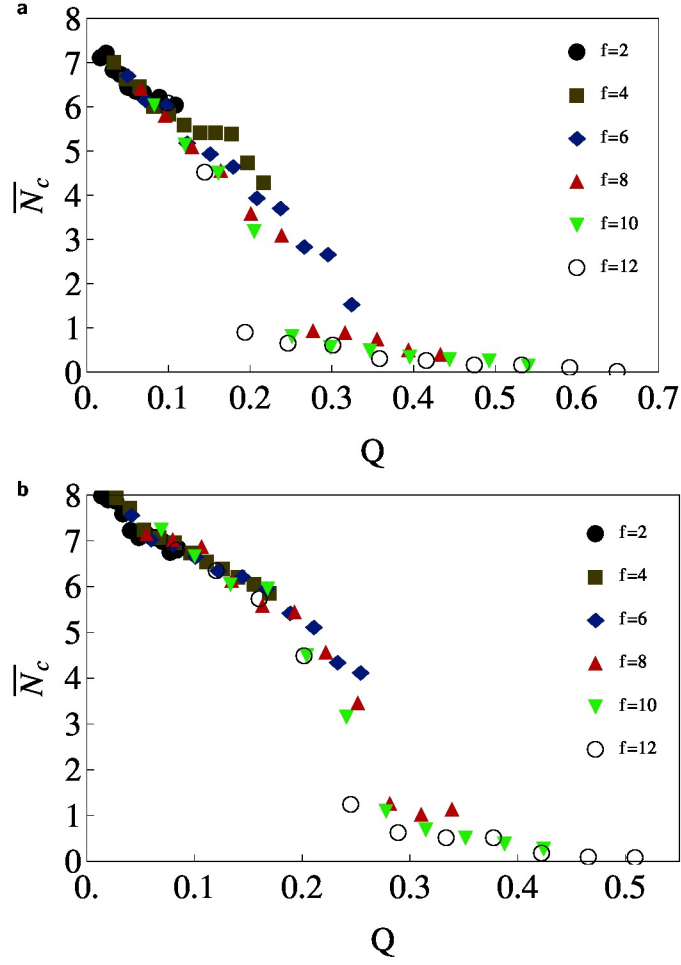
Extended Data Figure 3: Brightfield (left) and fluorescence (middle) microscopy images for variations on the FLA coupling method, and the fluorescence intensity on a horizontal line through the fluorescence maximum (right). Note the different scale in (a). a) Poly(styrene-*co*-acrylic acid) spheres activated and functionalized as described in Methods. b) Without EDC addition, fluorescence intensity is low, because the carboxylic acid groups are not activated. c) Without FLA addition, fluorescence intensity is almost undetectable. d) For activated and functionalized polystyrene spheres, fluorescence intensity is low, because no carboxylic acid groups are present. The higher fluorescence intensity for (d) compared to (b), can be explained because the hydrophilic hairs on CPSAA prevent adsorption of FLA on the particle surface. For the fluorescence microscopy images, the image levels are linearly rescaled, with lower level threshold at 0% and upper level threshold at 99.95% of (a).



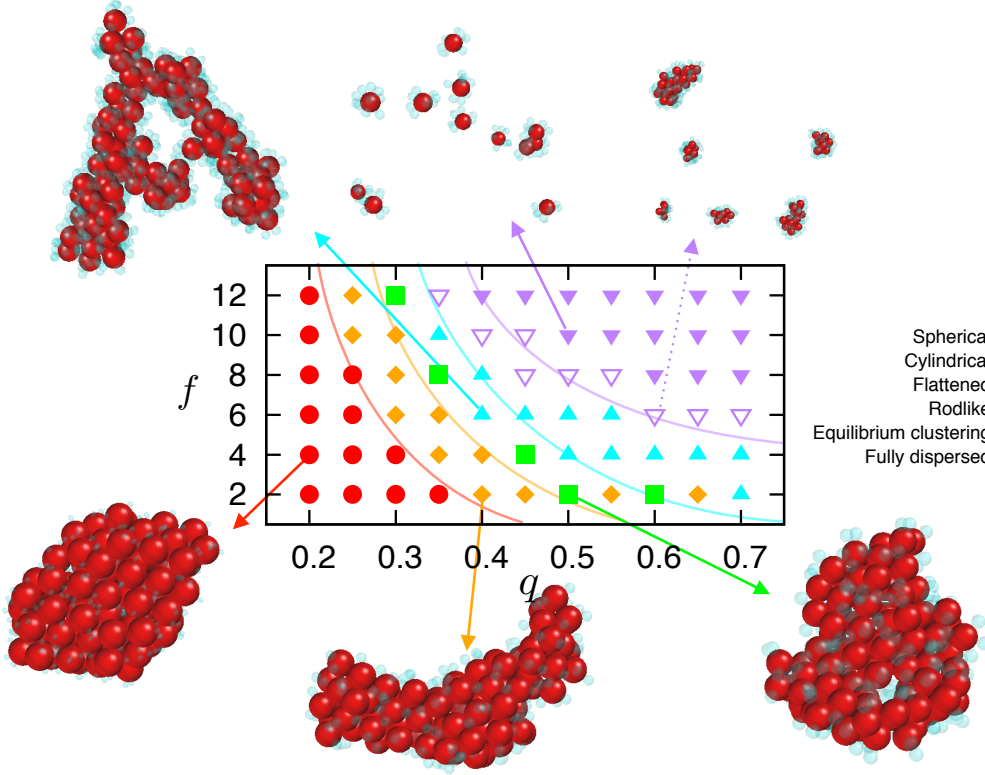
Extended Data Figure 4: *SEM images of sheets and shells.* SEM images after freeze-drying (a-c) and sintering (d-f). For both methods, sheets (a,d) and shells (b-c,e-f) are observed.



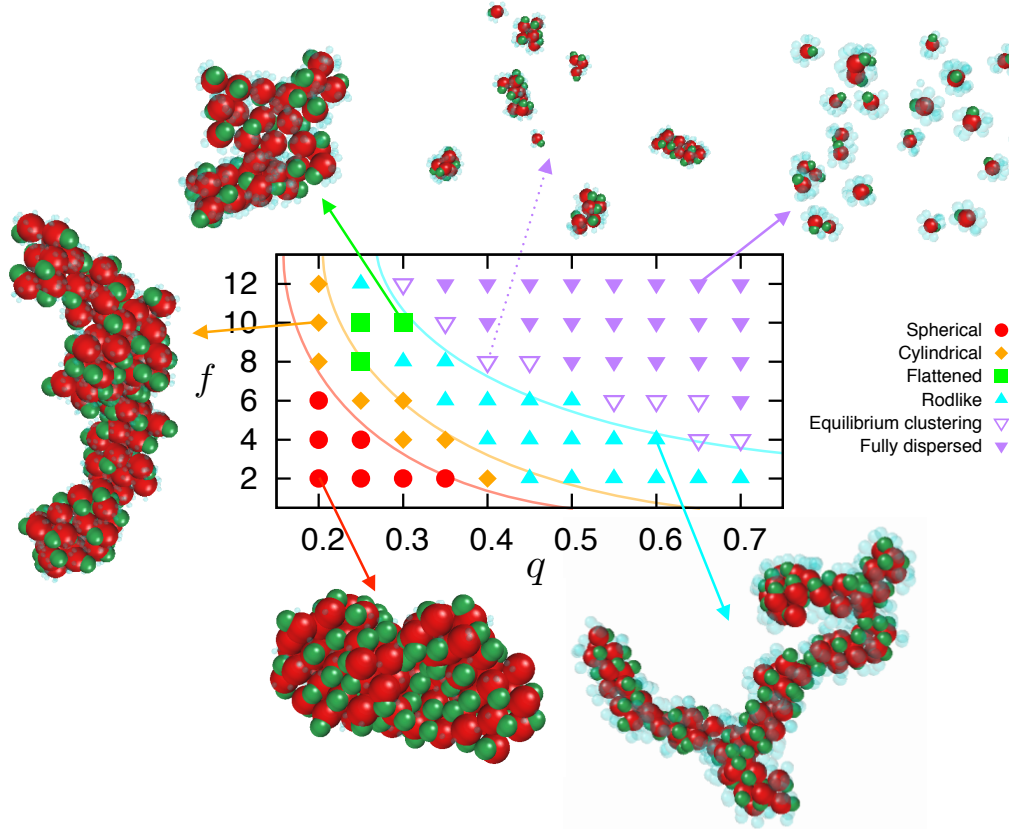
Extended Data Figure 5: *Sheets.* a) For floppy snowman-like particles with varying sizes (b-d), not only hollow shells (Fig. 2), but also two-dimensional crystalline sheets (f-h) are found using optical microscopy. Both tBA (e), and FlA (f-h) are used as hydrophobic moieties and for both moieties sheets are observed.



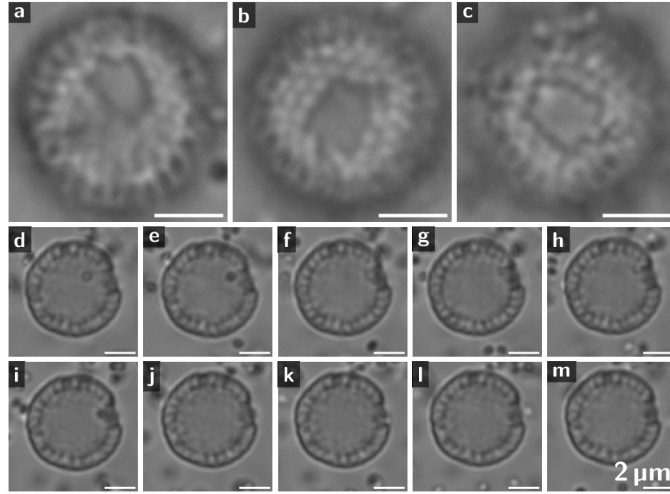
Extended Data Figure 6: *Average number of contacts per particle versus polymer surface fraction for simulations initiated from the soluble phase.* Plot of the average number of contacts \bar{N}_c versus polymer surface fraction for the soluble phase simulations with (a) and without (b) protrusions. Particles without protrusions form on average ~ 1 additional contact.



Extended Data Figure 7: *Morphology diagram for simulations of floppy spheres initiated from the soluble phase.* Representative simulation snapshots are shown for each morphology: spherical (red circles), cylindrical (orange diamond), flattened (green square), rodlike (blue filled upwards pointing triangle), equilibrium clustering (purple empty downwards pointing triangle) and fully dispersed (purple filled downwards pointing triangle). The coloured lines visualise the trends in morphology change, and indicate that the aggregate dimensionality reduces with increasing f and q .



Extended Data Figure 8: *Morphology diagram for simulations of floppy snowman-like particles initiated from the soluble phase.* Representative simulation snapshots are shown for each morphology: spherical (red circles), cylindrical (orange diamond), flattened (green square), rodlike (blue filled upwards pointing triangle), equilibrium clustering (purple empty downwards pointing triangle) and fully dispersed (purple filled downwards pointing triangle).



Extended Data Figure 9: Brightfield microscopy images of a shell with a large vacancy at a) $t = 0$, b) after one day, c) after five days. d-m) time series ($\Delta t = 88\text{ ms}$) of a single snowman-like particle inside the shell which escapes through the vacancy.